Review

Journal of
Nanoscience and Nanotechnology
Vol. 15, 959–971, 2015
www.aspbs.com/jnn

Nanodiamond-Based Composite Structures for Biomedical Imaging and Drug Delivery

Jessica M. Rosenholm[1,*], Igor I. Vlasov[2], Sergey A. Burikov[3], Tatiana A. Dolenko[3], and Olga A. Shenderova[4,5,*]

[1] *Laboratory for Physical Chemistry, Center for Functional Materials, Åbo Akademi University, FI-20500, Turku, Finland*
[2] *General Physics Institute, Russian Academy of Sciences, 119991 Moscow, Russia*
[3] *Moscow State University, 119991 Moscow, Russia*
[4] *International Technology Centre, Raleigh, North Carolina 27617, USA*
[5] *Adamas Nanotechnologies, Inc, Raleigh, North Carolina 27617, USA*

Nanodiamond particles are widely recognized candidates for biomedical applications due to their excellent biocompatibility, bright photoluminescence based on color centers and outstanding photostability. Recently, more complex architectures with a nanodiamond core and an external shell or nanostructure which provides synergistic benefits have been developed, and their feasibility for biomedical applications has been demonstrated. This review is aimed at summarizing recent achievements in the fabrication and functional demonstrations of nanodiamond-based composite structures, along with critical considerations that should be taken into account in the design of such structures from a biomedical point of view. A particular focus of the review is core/shell structures of nanodiamond surrounded by porous silica shells, which demonstrate a remarkable increase in drug loading efficiency; as well as nanodiamonds decorated with carbon dots, which have excellent potential as bioimaging probes. Other combinations are also considered, relying on the discussed inherent properties of the inorganic materials being integrated in a way to advance inorganic nanomedicine in the quest for better health-related nanotechnology.

Keywords: Nanodiamonds, Core/Shell, Mesoporous Silica, Cabon Dots, Biomedical Imaging, Drug Delivery.

CONTENTS

1. Introduction 959
2. ND/Silica Core/Shell Structures 961
2.1. Fabrication of Porous Shells 961
2.2. PL-ND as Core Materials 962
2.3. Biomedical Applicability 963
3. ND-Carbon Dot Structures 967
3.1. Fabrication of Carbon Dots Decorated Nanodiamonds (CDD-ND) 967
3.2. Properties of CDD-ND 968
4. Other Combinations 969
4.1. MSN-Carbon Dots Structure 969
5. Future Outlook 969
Acknowledgments 970
References and Notes 970

1. INTRODUCTION

One of the focus areas of nanomedicine involves the development of novel contrast agents with improved properties relative to existing imaging agents. The driver for this development is connected to problems associated with conventional imaging agents, e.g., fluorescent dye molecules which suffer from photobleaching over time, as well as instability in the biological/physiological environment and occasionally phototoxicity. While magnetic nanoparticles can be readily exploited as contrast agents for magnetic resonance imaging (MRI),[1] on the optical imaging side, fluorescent semiconductor nanoparticles (quantum dots, QD) have been put forward as promising bioprobes.[2–4] The most prominent property of QDs are high fluorescence quantum yield and narrow emission bands, which can moreover be carefully tuned over most of the visible-NIR spectral range by varying their size and chemical composition.[5–10] However, lately there have been concerns regarding their heavy metal composition, which may render the application of QDs rather limited due to their inherent toxicity especially for clinical applications.[11,12] Carbon-based materials, such as nanodiamonds (ND) and

*Authors to whom correspondence should be addressed.

carbon dots (CD), have consequently gained ground as promising, non-toxic alternatives to QDs. Similar to QDs, they have a high fluorescence quantum yield. The position of the emission band of CDs is tuned by changing their size and defect structures, whereas the emission band position of NDs depends only on the defect structure. The peak in the emission from CDs is in the blue-green range which is not optimal for imaging of live cells. This disadvantage of CDs is compensated by their high brightness and small sizes (down to ~ 2 nm). The brightest emission from ND, however, occurs in the green-red range depending on the structure of the defects produced in the ND core. The fluorescence intensity strongly increases with ND size, as larger size encompasses more color defects.[13, 14] One particularly advantageous aspect regarding ND photoluminescence when it comes to biomedical applications, is that the nitrogen-vacancy defect centers emit photons in the far-red/near-infrared region[15]

Jessica M. Rosenholm holds an adjunct professorship (title of docent) in Biomedical Nanotechnology at Åbo Akademi University, Finland, from where she also received her M.Sc. (Tech) degree in chemical engineering in 2002. Her doctorate period included a four-year funded position in the national Biomaterials and Tissue Engineering Graduate School, from which she graduated her D.Sc. (Tech) in materials science 2008. Her thesis work has been awarded national and international prizes, e.g., the Akzo Nobel Nordic Research Prize 2009 for best doctoral thesis and research activity in colloid and surface science in the Nordic countries. In 2009–2010 she spent a postdoctoral period at the Nano Biomedical Research Centre, Med-X Research Institute, Shanghai Jiao Tong University in China. Since then, she heads her own group, the BioNanoMaterials group (www.fyke.fi/bionano), at the Laboratory for Physical Chemistry at ÅAU. The group's activities are centred around the development of functional nanoparticles for detection, tracking, diagnostic and/or therapeutic biomedical applications, based largely on mesoporous silica and its composite nanostructures.

Igor I. Vlasov received an M.S. in physics from the Physics Department of Moscow State University in 1983. He joined the Vernadsky Institute of Geochemistry and Analytical Chemistry in 1983 where he carried out research on a new technique of atomic spectroscopy, Laser Enhanced Ionization (LEI) spectroscopy. He received a Ph.D. in physics in 1993 for development of the LEI spectroscopy for detection of ultra-low concentration of impurities in semiconductors. In 1995 he joined the General Physics Institute, where his interests include developing of advanced carbon nanomaterials for nanophotonics, quantum information processing, biomedicine. Now he is head of the group for laser spectroscopy of carbon materials. He pioneered the experimental and theoretical works on searching of smallest stably luminescent nanodiamonds.

Sergey A. Burikov Born 1978. Graduated in 2002 from Physical Department of M. V. Lomonosov Moscow State University. Candidate degree in physics and mathematics (2008). Senior research scientist in M. V. Lomonosov Moscow State University (Department of Physics). Author of more than 30 papers. Fellow of MSU Scholarship for talented young researchers and lecturers. Area of research: Raman and IR spectroscopy, aqueous solutions, colloidal solutions of nanoparticles, inverse problems.

Tatiana A. Dolenko Born 1961. Graduated *cum laude* in 1983 from Physical Department of M. V. Lomonosov Moscow State University. Candidate degree in physics and mathematics (1987). Senior research scientist in M. V. Lomonosov Moscow State University (Department of Physics). Since 2008, Tatiana is the Head of Group of laser spectroscopy of solutions of supramolecular compounds and nanostructures. Author of about 100 papers. Member of the Optical Society of Russia and of the Russian Association of Pattern Recognition and Image Analysis. Laureate of Lenin Komsomol Prize (1985). Area of research: Raman and IR spectroscopy, aqueous solutions, colloidal solutions of nanoparticles, inverse problems, artificial neural networks.

Olga A. Shenderova is the Head of the Nanocarbon Laboratory of the International Technology Center (ITC) and President of Adámas Nanotecnologies Inc., Raleigh, USA. She received her Ph.D. in Materials Science from the St. Petersburg State Technical University, Russia (1991). During her appointment at North Carolina State University (1995–2001) she performed atomistic simulations of mechanical and electronic properties of carbon nanostructures. Since 2001 she has worked at ITC on applied research projects in the areas of nanodiamond (ND) particle surface modification, influence of synthesis conditions on ND composition, nitrogen state in ND, development of ND-based additives for lubricants, ND-polymer composites, optical and biological applications of ND. She has given more than 100 invited talks and authored over 120 papers in peer reviewed journals, 15 book chapters, and edited 5 books related to nanodiamonds. She has 20 patents.

that efficiently penetrates tissue while being well separated from tissue and cellular autofluorescence.[16] For such applications, besides detectability, the same criteria applies to any nanoprobe intended for biomedical use, including controllable/well-defined particle size, shape, porosity and surface chemistry, well-dispersible particles which form colloidally stable suspensions (largely dictated by the particle size and shape, applied surface functionalization strategies, coatings, etc.), uniform, easily modifiable surface for further attachment of polymers (for steric stability, longer blood circulation times) and/or active moieties/targeting ligands (for specificity and controlled drug release mechanisms) and of course biocompatibility along with efficient clearance of the particles after tasks are completed (in the best case scenario, biodegradability).

The recent trend in the design of new nanomedicines involves nanoparticulate formulations that can combine drug delivery and imaging to allow for simultaneous diagnostics and therapy, often referred to as "theranostics." While this can be realized via many fabrication designs, one particularly attractive approach is the construction of core/shell materials where one construct is responsible for the imaging activity and the other for the drug incorporation. While inorganic nanostructures are already being readily utilized on the imaging side due to their inherent detectability by different imaging modalities,[17, 18] organic materials have advanced all the way to the market on the drug delivery side, e.g., liposomes for cancer therapy. The obvious choice for a theranostic probe would thus be construction of hybrid (organic + inorganic) materials to meet these demands. Nevertheless, taking advantage of the high chemical and mechanical stability along with the complex architectures of inorganic structures, inorganic/inorganic composites have also proven to be highly useful alternatives.[19–22] Such constructions often rely on core/shell designs, consisting of layers of two or more materials. Here, the two (or more) materials account for their own distinct functions, and/or a third material can be used to physically separate the other two materials which would otherwise lead to passivation of the activity of one of the materials (such as luminescence quenching), or the combination of two materials can in certain cases even enhance the properties of the other material. When it comes to theranostic agents, a popular core/shell design is constructed by the coating of optically/magnetically active materials (accounting for the diagnostic/imaging dimension) with porous silica shells (accounting for a high drug loading capacity due to its high porosity). Pioneered by Hyeon and coworkers in 2006, where hydrophobic iron oxide cores were coated with mesoporous silica shells,[23] thus resulting in a MRI-detectable drug carrier, this approach has since been applied to successfully coat inherently hydrophobic nanocrystals (iron oxides and QDs) with the aim of creating multifunctional (theranostic) agents.[24, 25] The synthesis protocol was later generalized to be applicable also for hydrophilic material cores,[26] whereby core/shell designs comprising a detectable core and porous shell for drug loading based on also manganese oxide[27, 28] (magnetic activity) as well as lanthanide-doped inorganic nanocrystals [Gd_2O_3:Eu^{3+}][29](optical activity) have also been recently fabricated for similar purposes.

2. ND/SILICA CORE/SHELL STRUCTURES

As discussed above, NDs can emit bright internal fluorescence in the red range related to nitrogen-vacancy defects (NV) in the crystal lattice, and since they are further photostable, non-toxic and have a high refractive index, they can be readily exploited for biomedical imaging. Another inorganic nanomaterial class, silica nanoparticles, has to date been studied extensively as drug carriers, especially in porous form.[30–36] Adapting the core/shell approach mentioned above, these two distinct functions of both ND and mesoporous silica nanoparticles (MSN) can similarly be exploited by integrating them into a composite material, ND@MSN, comprising a ND core coated with a mesoporous silica shell.[37] This novel composite nanomaterial has been investigated for its applicability as a multifunctional nanosized theranostic probe suitable for combined biomedical imaging and drug delivery[38] which will be more discussed in the following.

2.1. Fabrication of Porous Shells

The seeded growth process used to produce porous shells on other material cores is substantially different from the quite well-established syntheses of pristine mesoporous

silica nanoparticles (MSNs), in that it may differ in size control mechanisms and in which no seeded growth is taking place.[39] Mesoporous silica shells have to date been successfully deposited on solid cores consisting of a range of inorganic materials, e.g., platinum,[40,41] gold,[42–46] NaCl crystals,[47] quantum dots[23,44] and silver.[48] The mesoporous silica-coated composite material subject to the most extensive research is, however, beyond doubt MSNs comprising of a magnetic nanocrystal core, typically ferro- or superparamagnetic iron oxide (SPIO). These designs are mostly aimed towards rendering the nanocomposites suitable for MR-imaging, but also for allowing external control via an applied magnetic field to achieve magnetically controlled drug delivery, hyperthermia, or magnetofection.[49–51] In this case, the magnetic nanoparticles can be incorporated into the mesoporous silica via many fabrication strategies,[52] whereby coating a silica shell around the magnetic iron oxide nanocrystals to form a magnetic-core/silica-shell structure, is usually employed for production of materials with nanoscale morphology. The mesoporous layer can be deposited either directly onto the magnetic cores[31,53,54] or the magnetic crystals can be pre-coated[55–58] with a dense silica layer via the modified Stöber[59] process,[60] generally used to coat metal/metal oxide crystals with silica, whereas the subsequent mesoporous coating process would be equivalent to that of coating of silica surfaces.[61–63]

2.2. PL-ND as Core Materials

Coating of other materials with silica has long been regarded as versatile means of tailoring colloids and other nanostructures.[64] This mainly applies to non-porous silica coatings, though, whereas coating of nanoparticles with porous silica layers was not reported before 2006, and has since then been quite well established especially for hydrophobic core materials. However, the exact same coating regime is not applicable to hydrophilic cores. This is due to that the templating surfactant, cetyltrimethyl ammonium bromide (CTAB), which is used both as as a pore-templating agent as well as a phase-transfer agent from organic to aqueous solvent in the hydrophobic core synthesis; would intuitively be expected to arrange the other way around on a hydrophilic core, and thus rather promote precipitation from the aqueous phase for hydrophilic cores. There has been great efforts in the nanodiamond field to produce colloidal ND which can be readily dispersed especially in aqueous solvents.[65–70] Aqueous dispersibility is, obviously, crucial from any biomedical application point of view. Nanodiamonds of different origin are usually purified in strong acids after production. This process results in a range of different functional groups being created on the surface of the ND due to the oxidation of residual carbon. Thus, the surface charges recorded for ND range from highly positive to highly negative,[71] and no "general," characteristic surface charge exists. The majority of surface groups on NDs with negative charge are carboxylic acid groups resulting from oxidation. This property can be utilized to promote the self-assembly of the cationic CTAB micelles, serving as a template for the mesopores, directly onto the ND surface. Added silica species can subsequently co-assemble with the CTAB micelles, and condense to form an ordered silica (SiO_2) network as a result of a base-catalyzed reaction. Solvent properties control the reaction rate, and in parallel, also the coating thickness i.e., final nanocomposite particle size. Thus, the synthesis components are essentially the same as those employed for conventional MCM-41 synthesis: water, ammonia, CTAB as structure-directing agent and TEOS as a silica source, with the vital addition of ethanol when coatings on nanoscaled cores are the objective.[72,73] After separation from the synthesis mixture, the CTAB needs to be carefully removed, on the one hand, to liberate the pores i.e., to render the material porous, and on the other hand since being a cationic surfactant, it is toxic to living organisms. For conventional mesoporous materials this is readily accomplished by calcination at high temperatures, which would remove all organic material, but for nanoscaled materials solvent extraction methods are usually preferred due to better preservation of redispersibility using these approaches. The thickness of the resulting porous coatings, with radially aligned pores, can be tuned down to a couple of tens of nanometers by adjusting the water/ethanol ratio in the synthesis, thus enabling rational size control of the resulting composite particles.[37] Such a ND@MSN construct is depicted in Figure 1.

The challenge in coating of nanomaterials is to keep the cores separated during shell formation, in order not to end up with multiple cores in one composite, or the other way around, not having a core in all resulting particles. The challenge of obtaining well-dispersed ND, that would also be colloidally stable, has also been well-recognized by the ND community. The distinction between ND crystal size (derived from X-ray analysis) to that of the state of ND in solution (derived from dynamic light scattering) are crucial for the understanding of how the ND will behave throughout all processing steps such as surface functionalization, and all the way to application and further throughout the application lifecycle. The ND seldom

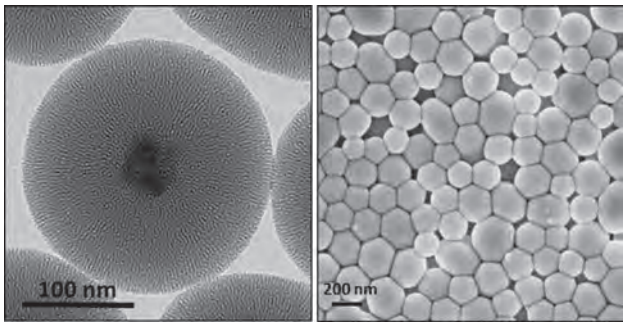

Figure 1. Electron microscopy images of ND@MSNs. Adapted with permission from [37], E. von Haartman, et al., *J. Mater. Chem. B* 1, 2358 **(2013)**. © 2013, The Royal Society of Chemistry.

present themselves as single ND crystals in solution, while the "standard" size usually reported is that of X-ray analysis that does not reveal the state and/or dispersibility of the NDs in solution. Microscopy techniques such as atomic force microscopy (AFM) and transmission electron microscopy (TEM) have also been applied to study the state of aggregation of ND upon drying on the AFM or TEM substrates, but do not necessarily reflect the state in solution, especially under non-optimized conditions. Here, we note that dynamic light scattering (DLS) data is crucial and even a requirement when claiming to have dispersed/colloidal ND, whereas X-ray can only reveal the individual crystal size of a powdered sample. Further, the conditions (solvent/pH/concentration/additives) during DLS measurement need to be defined, and the mode of analysis (such as size distribution model used) should also be stated to make measurements comparable. It should further be noted that DLS analysis is generally also dependent on the ultrasonication preparation procedure of the suspensions. Some recent efforts have thus involved the development of new tools for distinguishing the state of aggregation in dry and wet state of ND, and further tried to monitor the changes in state as a result of different types of treatment to increase the reproducibility of ND dispersity.[74] This approach is based on differential scanning calorimetry (DSC) of gels and powders of ND from which the dispersity could be estimated based on the Gibbs-Thompson equation, where ΔT represents the dispersity, and a strong correlation was found between DLS data for colloidal ND and DSC parameters for gels and powders of the same material.[74] Thus, this method should represent a solid way of defining the dispersity of ND that is unaffected by parameters such as temperature, pH and surface coverage of functional groups. For instance, the size of the primary crystallites in a detonation nanodiamond (DND) is typically 4–6 nm, while typical aggregate sizes in DND suspensions cover the size range 60–200 nm. In order for NDs to be applicable in biological systems, full dispersability of NDs is needed, especially so under aqueous conditions, since biological/physiological conditions always involve water. Thus, the application conditions in these cases are largely defined, including a specific pH ($\sim$7.4), temperature ($\sim$37 °C) and ionic strength (corresponding to 0.9 wt% or 0.15 M NaCl) which should also be taken into account when defining the colloidal stability during application. It should be noted that "full dispersibility" in terms of applicability does not necessarily mean that the NDs need to be dispersible as single crystals if such small sizes are not aimed for, but the state of aggregation need to be known/controlled. The state of aggregation determines the final ND (aggregate) size in solution, the size which is also determined by DLS as the hydrodynamic size, and size (along with surface charge) is one of the main determinants for the biobehavior of nanomaterials. Obtaining highly water dispersible ND requires effective methods allowing destruction of aggregates of DND to 20 nm size particles in water by chemical means,[75,76] complete disaggregation to 5 nm primary particle size in water by the bead milling technique[77] or direct laser-ablation based synthesis of ND particles in water with the particle size of several nm.[78,79] It should be noted that the surface chemistry of ND is also closely related to the resulting ND colloidal size, as the state of aggregation can be rapidly altered by changes in surface chemistry, which also depend on the surrounding conditions. Thus, a well-defined surface is also crucial for the prediction of the behavior of the ND system as a function of changes in the local environment as well as inter-particle interactions.[80,81]

Recently, Bumb et al. developed a liposome-based encapsulation process for coating of ND with non-porous silica that self-selects for a desired particle size and thus produces a monodisperse composite suspension.[82] Conventional silica-coating procedures for production of non-porous silica shells such as the microemulsion route may encounter some difficulties in coating of ND, where the core could be concentrated in the oil phase or the water phase depending on the nature of the ND surface. As a consequence, it may be hard to control the number of the cores encapsulated in the shell, especially for the case when one is aiming to generate single-core composite particles. Further, due to the microemulsion nature of the template, the particle size cannot be controlled to be in the smaller size range. In the liposomal encapsulation process, ultrasonication is used to break up the originally formed multilamellar vesicles to small unilamellar vesicles of approximately 100 nm size containing ND, in which the condensation of silica is base-catalyzed to produce a coating around the ND whereafter the lipid bilayer is removed (Fig. 2). The resulting ND-silica composite displayed the same advantages as the porous silica layers provided, i.e., reasonable colloidal stability, dispersability in aqueous solvent, as well as flexible and facile surface functionalization options, even though a precise particle diameter tuning may be more challenging in this case.[82]

2.3. Biomedical Applicability

2.3.1. Drug Delivery Carrier Design Aspects

Recent advances, especially based on the work of Ho and co-workers,[83] have also introduced ND as a potential nanomedical drug delivery platform. The drug delivery feature for ND systems is accomplished by covalent attachment[84,85] or physisorption[86,89] of therapeutic modalities. Nevertheless, the limited surface area of the ND, tendency for aggregation and exposed nature of the therapeutic modality, which might influence stability and therapeutic efficacy of the drug, can hamper the applicability of ND as optimal carriers for certain drugs. Here, the advantages of constructing a composite structure with distinct properties associated with each of the combined materials may offer some synergistic advantages. Considering the predecessor of the porous coatings, all-silica MSNs, the most prominent property of which as drug delivery carriers

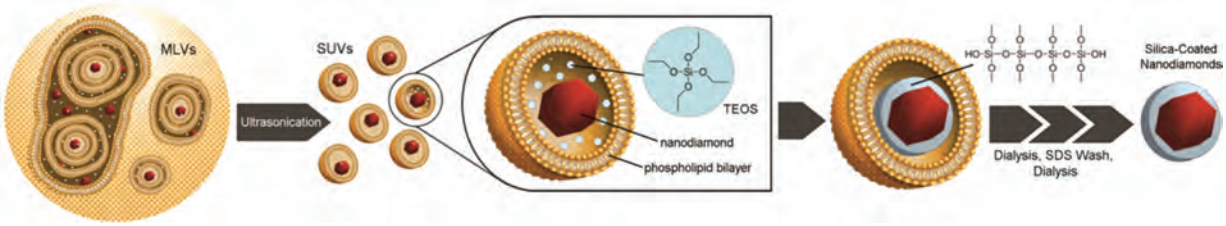

Figure 2. Synthesis of nonporous SiO_2-ND composites via a liposome-based encapsulation process. Nanodiamonds in a solution of tetraethyl orthosilicate (TEOS) are trapped in 1-palmitoyl-2-oleoyl-sn-glycero-3-phosphocholine (POPC) multilamellar vesicles (MLVs) that can range in size from 500 to 10000 nm. Ultrasonication breaks the MLVs into small unilamellar vesicles (SUVs) with nominal diameters of ~100 nm. TEOS is converted into silica, catalyzed by triethylamine (TEA). Thereafter, free TEOS and TEA are dialyzed away. A sodium dodecyl sulfate (SDS) wash breaks up the liposomes to free the coated nanodiamonds, and the remaining reagents (i.e., SDS and POPC) are removed by dialysis. Reprinted with permission from [82], A. Bumb et al., *J. Am. Chem. Soc.* 135, 7815 **(2013)**. © 2013, American Chemical Society.

is their high loading capacity, stemming from the characteristic high specific surface areas (up to ≥1000 m^2/g) and pore volumes. Silica is a well-known adsorbent with a high affinity towards a range of guest molecules, in drug delivery context especially suitable for hydrophobic drug cargo, that is generally challenging to formulate. With ~40% of the drugs on the market and ~90% of drugs in the development pipeline being poorly soluble in water,[90] a significant number of drug molecules fall into this category. There are extensive examples in the literature of examples where (pure) mesoporous silica has been used as drug carriers[30–36] and a solid core will certainly not change this inherent property of the coating.

When establishing general and/or mechanistic relationships with regard to drug loading capacity and/or release, model drugs are often utilized. When studied in a biological setting, fluorescent dyes are especially advantageous to use as model drugs, as the drug release process can in this case be studied live and inside cells. Thus, the capability of all-silica MSNs to release entrapped cargo intracellularly has been studied *in vitro* e.g., using the hydrophilic (water soluble) fluorescent dye calcein[91] or hydrophobic (poorly soluble) carbocyanine dyes[92] as model drugs. Notably the anticancer drug doxorubicinis also fluorescent, and therefore also probably the most frequently used model drug in nanomedical context. Albeit this molecule is quite water-soluble, and cannot consequently be used to draw conclusions for the behavior of poorly soluble drug cargo. Measuring the drug efficacy can often be challenging and requires elaborate biological assays, and thus the use of dyes can provide a more quantitative measure and easier methods of determination of delivery efficiency and kinetics in the early stages of carrier development.[108] Cell viability is an often applied method to determine particle-mediated delivery in biomedical context, but this approach largely limits the choice of drug to cytotoxins. However, as about two-thirds of nanomedical drug delivery products are aimed at cancer therapy, this could still be highly relevant in context, if the drug efficacy can easily be determined *in vitro* with the aid of cell viability assays. On a more general level, if the drug carrier properties are evaluated rather than the action of a specific formulation, this kind of experiment may, however, rather provide information on the action of the specific drug than any generic drug release mechanism brought upon by the carrier platform. It would also be limited in providing any information on the kinetics, localization, or intracellular distribution of the drug after release. For fluorescent cargo, fluorescence-based techniques can be utilized to study the drug release process as well as the intracellular delivery efficiency. Consequently, the drug release process can be followed real-time by live cell imaging, which can allow for the determination of localization of release (intra/extracellular, compartmentalization, etc.) and subsequent intracellular distribution of cargo by microscopy, and furthermore, the delivery efficiency can be determined by either image analysis (lower *n* of sampling) or fluorescence-assisted cell sorting (high *n* of sampling, generally 10^4 cells is used). When a specific drug-carrier formulation is sought for and/or the formulation will be evaluated on a disease model which has been well established for a specific drug, using the actual drug in question will naturally provide the most valuable information.

When loaded with a hydrophobic cargo, the choice of the right surface chemistry becomes increasingly important. Even though the inherent material would be hydrophilic, depending on the loading mechanism of the drug cargo, the hydrophilic surface may be rendered hydrophobic when covered up by hydrophobic molecules in large amounts.[93] For mesoporous silica structures, the loading of the cargo takes place by utilizing the enormous surface areas (up to ≥1000 m^2/g) to adsorb drug molecules under conditions where favorable interactions between surface and cargo molecules can occur.[93] For ND@MSN, loading degrees of ≥100 wt% (drug/carrier) have been reported for the red carbocyaninedye DiI, with similar loading degrees obtained for hydrophobic drugs (dexamethasone, furosemide, and prednisolone).[37] Loading of large amounts of hydrophobic cargo can thus decrease the redispersablity of the inherently hydrophilic particle, whereby coating the consequently hydrophobized loaded particle with a second hydrophilic layer can restore the hydrophilicity of the system.[38] The sequence of ND@MSN composite construction via drug loading and final surface coating accounting for this phenomena

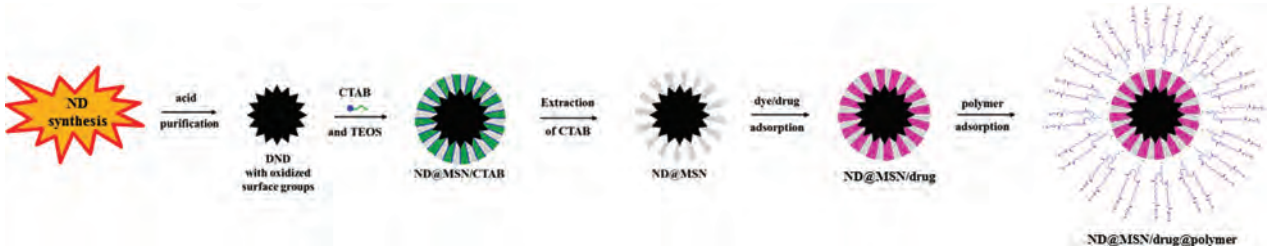

Figure 3. Overview of the coating of ND cores with porous silica shells, subsequent cargo loading and finally organic modification of the loaded composite particle. Courtesy of Eva von Haartman.

is illustrated in Figure 3, with applicability demonstrations of the same below.

2.3.2. Detectability in a Biological Setting

Similarly as size by XRD/SAXS, also ND photoluminescence is generally measured in the powder state. When imaged in a biological setting, as high laser powers as used for samples of pure material cannot be used, in order to avoid destroying the cells/organisms. Due to this reason, most studies reporting on biomedical applications of ND to date have used additional fluorescent labels to detect the ND in a biological setting. However, the same problems as for all other nanoparticulate systems connected to the properties of the used organic fluorophores are thus encountered, such as inhomogeneous incorporation of fluorophores (variation in fluorescence intensity), photoinstability, phototoxicity, variability in fluorescence properties depending on the environment (intra/extracellular pH, presence of quenching agents, hydrophobicity/hydrophilicity e.g., membranes/cytosol) as well as the possibility of fluorophore detachment (hydrolysis, enzymatic) leading to uncertainty whether it is free fluorophore or particle system that is being traced. The latter risk is imminent especially if the fluorescent tag was attached by physical adsorption only, but it should be pointed out that also covalent attachment does not guarantee stability in the physiological environment due to the abovementioned reasons. Thus, it should be evident that the inherent PL of ND should be utilized in order to gain an edge against existing nanoparticle systems relaying on attachment of fluorescent tags.

NDs have to date been studied in biological settings utilizing a range of different techniques, including Raman scattering, reflection, stimulated emission-depletion microscopy (STED) and of course fluorescence microscopy, including multiphoton microscopy (Fig. 4).

As for all cellular labels, the challenge lies in obtaining adequately high sensitivity and signal strength, and thus the labeling efficiency i.e., cellular uptake of label (particle serving as imaging agent) should be sufficient. The key properties for achieving this are (a) proper dispersability in the biological media and (b) suitable surface coating and/or charge that facilitates cellular uptake. To attain this, inorganic materials are often organically modified, as organic functionalization provides for very flexible design alternatives (including stimuli-responsive drug delivery systems) and further, can even enhance the biocompatibility of the system (c.f. QDs[12, 94]). Inorganic functionalization in the form of silica coating can also provide similar advantages, as amorphous silica is a hydrophilic material and can thus promote water-dispersibility, is further an endogenous substance and thus known for its biocompatibility followed by biodegradability. Additionally, the (organic) functionalization of silica surfaces have been studied for several decades, whereas addition of a silica coating, let it be porous or non-porous, allows for further surface modification via all methods developed for silica; including surface grafting of functional silanes, polymer coating, ion doping, covalent linking of complexes, and co-condensation. The isoelectric point (IEP) for silica being 2–3 means that silica is negatively charged at physiological pH, whereas a positive charge have been found to be facilitative from a cellular uptake point of view. Thus, modification of the silica surface with positively charged groups would generally enhance the internalization by cells as compared to non-functionalized counterparts.[95] Here, amino-functionalized surfaces are among the most attractive surface modifications for biomedical applications, since amino groups bind strongly to several functional groups found in molecules of biological interest, and can easily be further conjugated with to active molecules using standard bioconjugation protocols. Poly(ethylene imine), PEI, is a hyberbranched polymer providing for the highest amount of primary amino groups. In the case of ND, PEI can be introduced either by grafting,[96, 97] or electrostatic adsorption[98] provided the ND is negatively charged at the adsorption conditions, or more efficiently, when mediated by a porous silica layer.[38, 108]

In drug delivery context, as discussed above (Section 2.3.1), hydrophilic polymeric coatings can further be critical especially for restoring the hydrophilicity of the carrier system when loaded with large amounts of hydrophobic cargo (Figs. 5(a), (b)). In this particular example, the polymer consisted of two components: the above-mentioned PEI co-polymerized with poly(ethylene glycol), PEG.[109] PEI can function as an anchor to the negatively charged particle surface, simultaneously imparting the particle system with an overall positive charge; allowing the hydrophilic but non-charged PEG chains to stick out into the solution. PEG is probably the

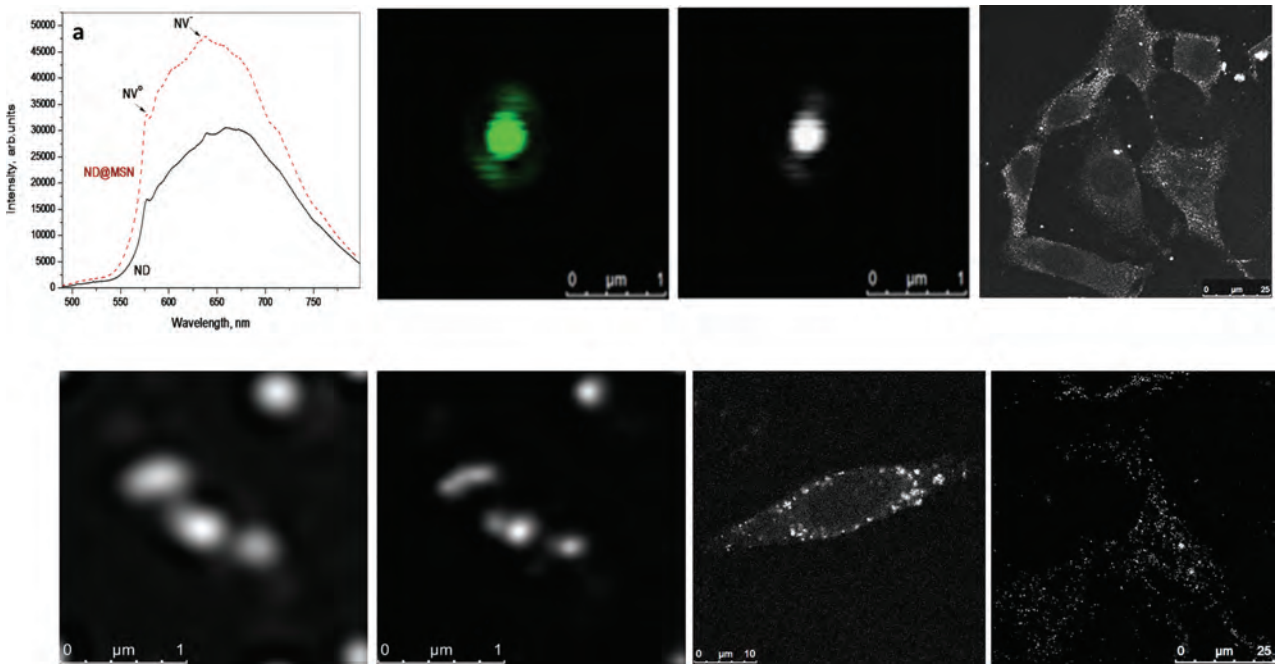

Figure 4. ND and ND@MSN composites imaged by different techniques. (a) Photoluminescence (PL) spectra of pure ND (solid line) and ND@MSN (dashed line). (b) Reflection image and (c) PL image of ND@MSN (d) Reflection from ND in HeLa cells. (e) Confocal and (f) STED image of ND. (g) PL image of HeLa cells with ND@MSN@PEI-PEG. (h) Two photon-imaging of ND in HeLa cells. [Reflection Channel : 500–550 nm. Photoluminescence Channel 650–730 nm.] Adapted with permission from [38], N. Prabhakar, et al., *Nanoscale* 5, 3713 **(2013)**. © 2013, The Royal Society of Chemistry.

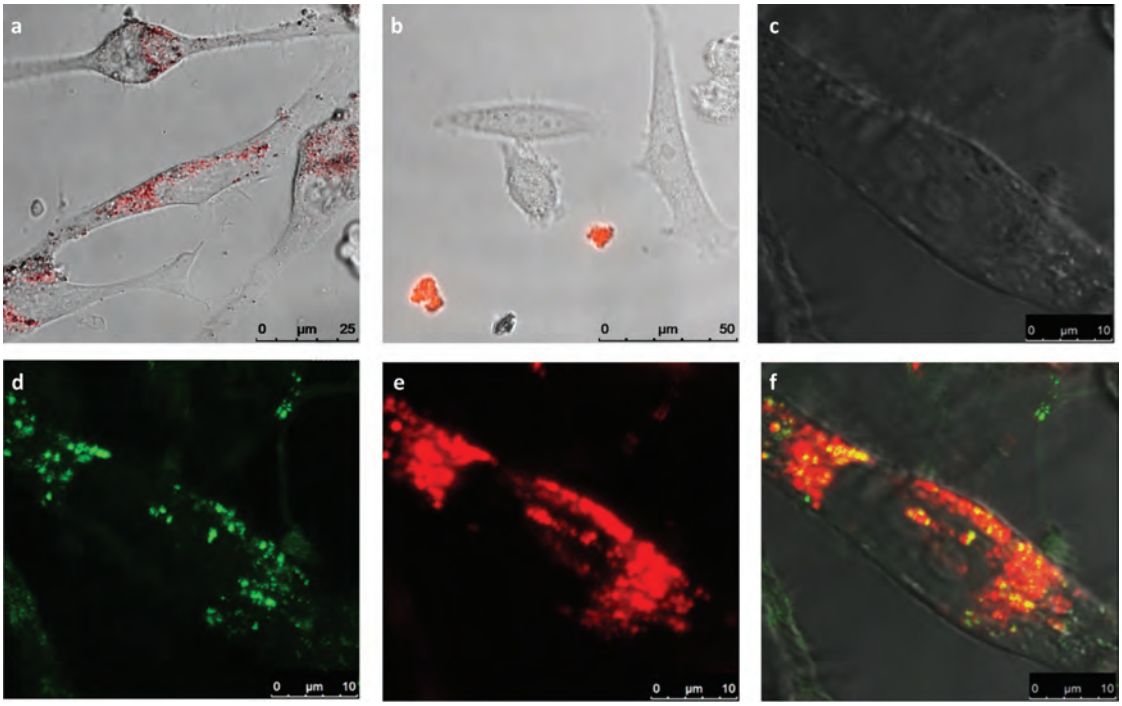

Figure 5. Intracellular delivery of model drugs by ND@MSNs. (a) Live cell image shows the permeation of copolymer-coated ND@MSNs (ND@MSN@PEI-PEG) loaded with 10 wt% DiI dye as cargo. (b) The uncoated ND@MSNs loaded with 10 wt% DiI dye forms aggregates and permeability is reduced. Intracellular release of ND@MSN@PEI-PEG loaded with DiI dye in HeLa cells after 72 h incubation: (c) a HeLa cell (d) Reflection image (in green) showing the internalization of ND@MSN@PEI-PEG particles, e) intracellular release of DiI dye (in red) from particles (f) overlay image. Adapted with permission from [38], N. Prabhakar, et al., *Nanoscale* 5, 3713 **(2013)**. © 2013, The Royal Society of Chemistry. Image collation courtesy of Neeraj Prabhakar.

mostly employed polymer coating in biomedical context, frequently used as a strategy to decrease opsonisation by plasma proteins and thus decrease recognition by the body's defense mechanisms, consequently improving the retention time *in vivo*. In the present case, the colloidal stability is improved by the steric stabilization provided by PEG combined with the electrostatic stabilization provided by PEI, while PEI may further aid in the endosomal escape of cargo after release (Fig. 5).

2.3.3. Theranostic Probes

For the delivery of drugs, reaching the right cell is not usually sufficient, as also the right intracellular target for the drug should be accessed. Many drugs need to reach the cytoplasm to exert their activity. Also here, the right choice of surface coating can aid in the process. PEI is known for its ability to destabilize endosomal membranes and thus promote endosomal escape thorugh the 'proton sponge' effect, which is why PEI is widely utilized also in gene delivery as an effective non-viral gene carrier when complexed with nucleic acids.[99, 100] For studying of this process, separate detection of carrier system and drug cargo is vital, whereby the advantages of using fluorescent model drug cargo should be evident. As for the carrier system, core/shell designs (where the core accounts for the tracing function) is the ultimate structure for the following of intracellular fate of the particles, since there is no risk of detached labels being traced instead of the particle itself. This constitutes a theranostic carrier, which not only provides a therapeutic aspect but also allows for follow-up of the drug delivery process, and this is also where photoluminescent nanomaterials hold great promise (see Fig. 6).

3. ND-CARBON DOT STRUCTURES

3.1. Fabrication of Carbon Dots Decorated Nanodiamonds (CDD-ND)

Recently it was demonstrated that a 3:1 sulfuric to nitric acid mixture can be used to produce photoluminescent (PL) carbon nanostructures by oxidation of micrographite, nanographite and other graphitic source materials at temperatures exceeding 100 °C.[101, 102] Oxidation of graphitic carbon using sulfuric and nitric acid is most efficient using a 3:1 ratio of sulfuric acid to nitric acid, as shown in the following reaction:

$$24nC + 3H_2SO_4 + HNO_3 = C^+_{24n}HSO_{4^-} \cdot 2H_2SO_4 + H_2O + NO_2$$

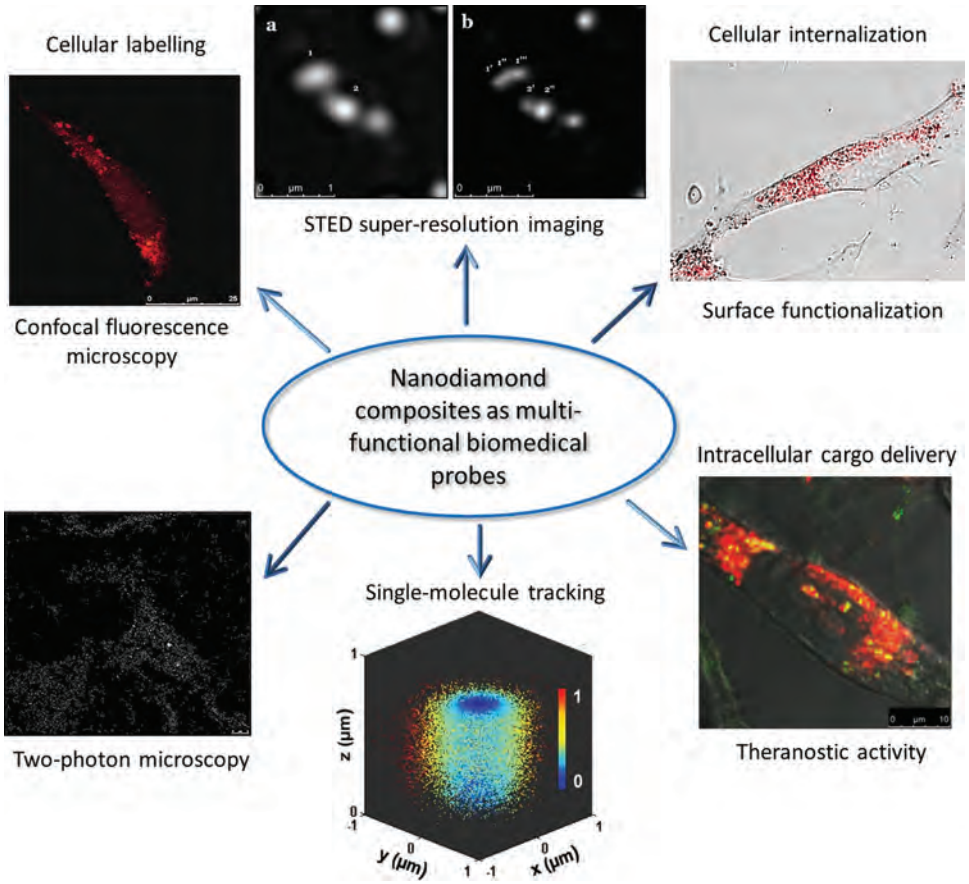

Figure 6. Overview of the versatility of nanodiamond composite materials in biomedicine. Adapted with permission from [82], A. Bumb, et al., *J. Am. Chem. Soc.* 135, 7815 **(2013)**. © 2013, American Chemical Society; and from [38], N. Prabhakar, et al., *Nanoscale* 5, 3713 **(2013)**. © 2013, The Royal Society of Chemistry. Image collation courtesy of Neeraj Prabhakar.

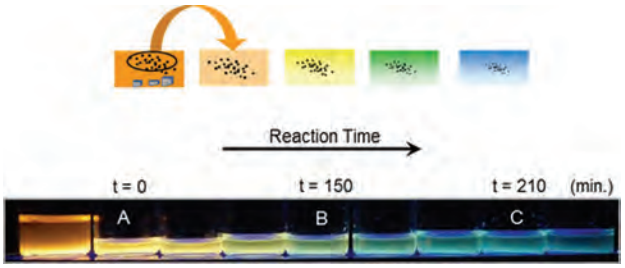

Figure 7. Time-dependence of PL color and intensity of the supernatant is shown for the reaction product of micrographite. A photograph of the yellow starting solution, solution A, along with supernatant aliquots taken at 30 minute intervals during the reaction of 3:1 acid mixture at 128 °C, illuminated with a 365 nm UV lamp. Adapted with permission from [101], S. C. Hens, et al., *J. Phys. Chem. C* 116, 20015 **(2012)**. © 2012, American Chemical Society.

where C is the graphitic compound and n is the stage index. This mixture functions as an exceptional graphite intercalation compound (GIC) which facilitates oxidation that initially forms graphite oxide followed by graphene oxide produced by exfoliation. This treatment produces colloidal supernatant solutions that are photoluminescent across the visible wavelength range. It was possible to tune the PL emission of the reaction suspension from the blue to red by tuning the combination of reaction temperature and time (Fig. 7). A similar treatment was applied to detonation soot,[101] which is the initial product of the detonation of carbon-containing high energy explosives from which purified ND is routinely derived on a large scale. Detonation soot consists of a mixture of chemically bonded nanodiamond and graphitic carbon phases. A starting sample of detonation soot in the 3:1 sulfuric/nitric acid mixture has a characteristic black color due to the presence of sp^2 carbon. The color changes from black to grey as a result of oxidation of the non-diamond carbon component in the soot producing a grey purified ND powder. Surprisingly, the ND possess a bright red PL after washing the grey colored NDs to remove the acid once the reaction is complete (Fig. 8). Under inspection in a high resolution transmission electron microscope (HRTEM), rounded sp^2 carbon species (carbon dots) bonded to the surface of ND particles were discovered, which are 1–2 atomic layers thick and 1–2 nm in lateral dimensions (Fig. 8, HRTEM image).[102] As was the case in the previous study,[101] oxidation of the sp^2 phase of the soot with the acid mixture results in the production of graphene\graphite oxides structures. The transparent supernatant, free of ND particles, has a light-yellow color in white light and very bright yellow-orange PL under UV illumination (Fig. 8). This color is characteristic of graphite/graphene oxide (GO) nanoparticles.[101] A schematic representation of the process and resultant products is shown in Figure 8.

3.2. Properties of CDD-ND

CDD-ND demonstrates surprisingly strong red photoluminescence. PL spectra measured for dry powders of

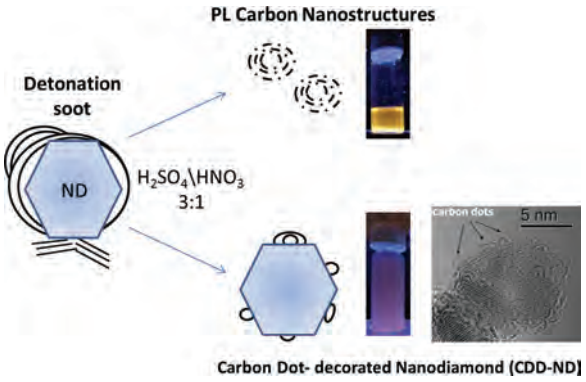

Figure 8. Schematic representation of the formation of PL products by treatment of detonation soot in a mixture of 3:1 sulfuric/nitric acids: carbon dots decorated ND produced from the diamond phase of the detonation soot (bottom) and free standing PL nanocarbon structures including carbon balls, formed by oxidation of the non-diamond carbon in the soot (top). Will be adapted with permission from [103], O. Shenderova, et al., Particle Part. Systems Character, DOI 10.1002/ppsc.201300251 **(2013)**. © 2010, WILEY-VCH Verlag GmbH & Co.

CDD-NDs treated at various time are shown in Figure 9. The integral PL intensities appeared to be 10 to 20 times stronger for the samples as compared to the well-purified DND (bottom line of the Fig. 9). It can also be concluded from Figure 9 that it is possible to maximize the PL emission by choosing the proper treatment time (at a fixed temperature). The maximum intensity of the emission was observed for a sample treated for 2 hrs at 115 °C. Higher temperature and longer time of treatment leads to essential decreased sample luminescence. In order to obtain intense photoluminescence for the treated samples, the reaction needs to be stopped before all sp^2 carbon has been fully oxidized. The PL intensity stability of the suspensions containing PL graphene\graphite oxide (Fig. 7) obtained by oxidation of nanographite and CDD-ND were compared to the photostability of a suspension of organic dye Alexa Fluor, under prolonged laser irradiation. All carbon-based samples demonstrated a highly stable PL, while the

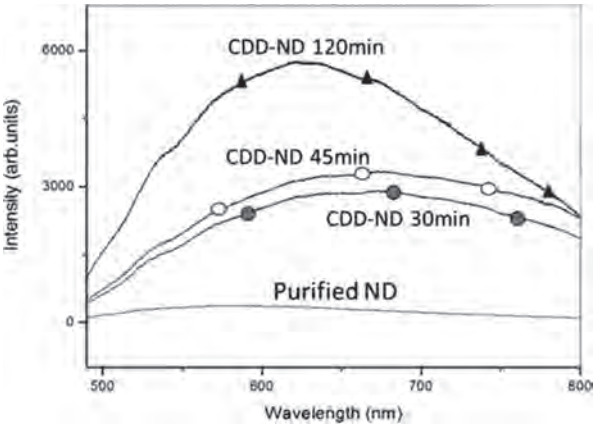

Figure 9. Fluorescence emission spectra for purified detonation ND and for the CDD-ND produced at different reaction times. The excitation wavelength is 488 nm.

intensity of the Alexa sample decreased by 45%.[102] Deviation from the average of the integral PL intensity was 3–4% for the CDD-ND and the nanoGO samples, and 6–8% for the well purified DND samples.

Conceptually, production of CDD-ND demonstrates synergistic benefits from joining two nanostructured materials in a single synthesis approach. The novel nanostructures composed of two nanocarbon materials, nanodiamonds and carbon dots, combine unique photophysical properties of both nanocarbons, greatly expanding their potential applications not achievable when the two nanocarbons exist separately. For example, bright red emission due to carbon dots can be combined with cathodoluminescent[103] or photoacoustic[104] imaging by creating structural defects in the diamond core, rendering CDD-ND with multimodal imaging properties. Similar to NDs, CDD-ND can serve as carriers for specific drug delivery along with imaging modality. Due to the facile production method, CDD-ND are inexpensive and can be used in large scale applications such as bio-related nanocomposites. In fact, their cost can be similar to the cost of detonation nanodiamonds annually produced in tons quantity. Using CDD-ND in compositions with biodegradable polymers would provide both reinforcement and photoluminescent monitoring of the polymer condition in tissue scaffold applications.[105]

4. OTHER COMBINATIONS

4.1. MSN-Carbon Dots Structure

Even though not comprised of any ND, another composite structure closely related to the other structures discussed in this paper is worth mentioning. This inorganic composite is based on all-silica MSNs capped with CDs as molecular gating systems.[106] Here, the authors took advantage of the residual carboxylic acid (COOH) groups on the surface of the CD, imparting them with a negative surface charge at physiological pH, and complexed them with amino-functionalized MSNs (NH_2-MSN) via electrostatic interactions (Fig. 10). Also taking advantage of the high loading capacity of MSNs, the anticancer drug doxorubicin could be loaded inside the pores, and thus kept in by the CD-gates under conditions where the caps and the carrier were oppositely charged. However, at intracellular pH, in the endo-lysosomal compartments, where nanoparticles generally end up as a result of endocytosis, the pH is acidic, around 5. In the presence of excess protons, the carboxylic acid groups of the CDs can protonate, and thus become non-charged ($COO^- \rightarrow COOH$) whereby the electrostatic interaction between the carrier and caps are lost, the caps are removed and the drug cargo can consequently be efficiently released from the MSN carrier (Fig. 10). This releasing effect was also observable when the MSN-CDs were incubated with HeLa cancer cells, whereby the drug efficacy in terms of decreased cell viability could be observed for the drug-loaded MSN-CD over free doxorubicin especially at higher concentrations. Consequently, not only could the CDs serve as pH-responsive molecular gates in this composite structure, but further impart the particle system with luminescent properties. Thus, in the same study, the authors also investigated the composite material's detectability both *in vitro* and *in vivo*, in the first case by incubating the composites with HeLa cancer cells followed by fluorescence microscopy imaging and in the latter case via subcutaneous injection of the particle suspension into the back flank area of nude mice, followed by imaging by an *in vivo* imaging system. The CD PL signal was clearly detectable in both cases, whereby the authors highlighted the potential of the developed system for non-invasive *in vivo* tracking combined with on-demand drug delivery of therapeutic agents to low-pH tissues such as tumors.[106]

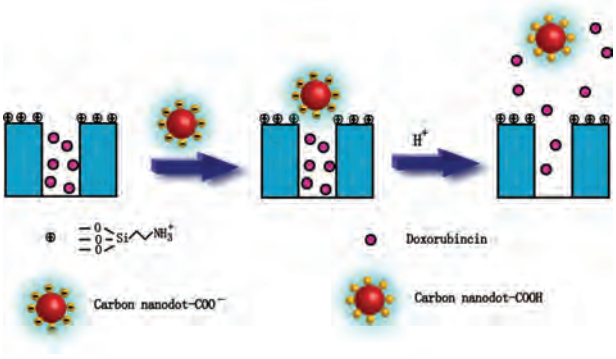

Figure 10. Carbon Dots as pH-sensitive pore gating systems in an MSN@CD composite structure. Published with permission from [106], L. Zhou, et al., *Langmuir* 29, 6396 **(2013)**. © 2013, American Chemical Society. DOI: 10.1021/la400479n.

5. FUTURE OUTLOOK

In the current review, some recent advances in the construction of inorganic nanocomposites comprising carbon nanostructures (ND or CD) as one of the components were presented. These composites have been designed in order to attain synergistic qualities to the resulting material, taking advantage of mainly the bright and stable photoluminescence of carbon materials and combining with other inorganic materials, in the present case silica. The added value properties introduced by these constructs have included:

(1) a well-defined particle morphology, size and/or surface chemistry that can be easily further modified if desired,

(2) a prominent drug loading capacity that can further be attained using established protocols, also comprising controlled-release mechanisms if desired,

(3) significant enhancement of the photoluminescence by the combination of materials, and

(4) a pH-responsive controlled-release mechanism triggered by conditions relevant for the intended application (inside cancer cells/tumors).

Such combinations of materials with distinct advantages could benefit greatly from each other and aid in pushing

inorganic nanomedicine further as a field, especially given the previous success of porous silica-coated magnetic nanoparticles.

Acknowledgments: We greatly acknowledge the funding from The Academy of Finland projects #137101, 140193, 260599 (Jessica M. Rosenholm). The authors further acknowledge funding from President's grant for leading scientific schools no. 3076.2012.2 (Igor I. Vlasov), and from Russian Academy of Sciences, program no. 24 (Igor I. Vlasov).

References and Notes

1. H. B. Na, I. C. Song, and T. Hyeon, *Adv. Mater.* 21, 2133 (**2009**).
2. X. MIchalet, F. F. Pinaud, L. A. Benrolila, J. M. Tsay, S. Doose, J. J. Li, G. Sundaresan, A. M. Wu, S. S. Gambhir, and S. Weiss, *Science* 307, 539 (**2005**).
3. I. L. Medintz, H. T. Uyeda, E. R. Goldman, and H. Mattoussi, *Nature Mater.* 4, 435 (**2005**).
4. B. Mahler, P. Spinicelli, S. Buil, X. Quelin, J. P. Hermier, and B. Dubertret, *Nature Nanotech.* 7, 659 (**2008**).
5. P. Reiss, M. Protière, and L. Li, *Small* 5, 154 (**2009**).
6. F. O. Silva, M. S. Carvalho, R. Mendonça, W. A. Macedo, K. Balzuweit, P. Reiss, and M. A. Schiavon, *Nanoscale Research Letters* 7, 536 (**2012**).
7. Y. Ghosh, B. D. Mangum, J. L. Casson, D. J. Williams, H. Htoon, and J. A. Hollingsworth, *J. Am. Chem. Soc.* 134, 9634 (**2012**).
8. F. García-Santamaría, S. Brovelli, R. Viswanatha, J. A. Hollingsworth, H. Htoon, S. A. Crooker, and V. I. Klimov, *Nano Lett.* 11, 687 (**2011**).
9. M. Grabolle, J. Ziegler, A. Merkulov, T. Nann, U. Resch-Genger, and N. Y. Ann, *Acad Sci.* 1130, 235 (**2008**).
10. J. Vela, H. Htoon, Y. Chen, Y.-S. Park, Y. Ghosh, P. M. Goodwin, J. H. Werner, N. P. Wells, J. L. Casson, and J. A. Hollingsworth, *J. Biophoton.* 3, 706 (**2010**).
11. C. Kirchner, T. Liedl, S. Kudera, T. Pellegrino, A. M. Javier, H. E. Gaub, S. Stolzle, N. Fertig, and W. Parak, *Nano Lett.* 5, 331 (**2005**).
12. L. Wang, D. K. Nagesha, S. Selvarasah, M. R. Dokmeci, and R. L. Carrier, *J. Nanobiotechnology* 6, 11 (**2008**).
13. S. N. Baker and G. A. Baker, *Angew. Chem. Int. Ed.* 49, 6726 (**2010**).
14. J.-H. Liu, S.-T. Yang, X.-X. Chen, and H. Wang, *Current Drug Metabolism* 13, 1046 (**2012**).
15. Y.-R. Chang, H.-Y. Lee, K. Chen, C.-C. Chang, D.-S. Tsai, C.-C. Fu, T.-S. Lim, Y.-K. Tzeng, C.-Y. Fang, C.-C. Han, H.-C. Chang, and W. Fann, *Nat. Nanotech.* 3, 284 (**2008**).
16. X. He, K. Wang, and Z. Cheng, *WIREs Nanomed. Nanobiotechol* 2, 349 (**2010**).
17. A. Taylor, K. M. Wilson, P. Murray, D. V. Fernig, and R. Lévy, *Chem. Soc. Rev.* 41, 2707 (**2012**).
18. S. Bhattacharyya, R. A. Kudgus, R. Bhattacharyya, and P. Mukherjee, *Pharm. Res.* 28, 237 (**2011**).
19. M. Arruebo, *WIREs Nanomed. Nanotechnol* 4, 16 (**2012**).
20. B. S. Sekhon and S. R. Kamboj, *Nanomedicine: NBM* 6, 516 (**2010**).
21. B. S. Sekhon, and S. R. Kamboj, *Nanomedicine: NBM* 6, 612 (**2010**).
22. M. Malmsten, *Current Opinion in Colloid and Interface Science* 18, 468 (**2013**).
23. J. Kim, J. E. Lee, J. Lee, J. H. Yu, B. C. Kim, K. An, Y. Hwang, C.-H. Shin, J.-G. Park, J. Kim, and T. Hyeon, *J. Am. Chem. Soc.* 128, 688 (**2006**).
24. J. E. Lee, N. Lee, T. Kim, J. Kim, and T. Hyeon, *Acc. Chem. Res.* 44, 893 (**2011**).
25. J. Zhang, J. M. Rosenholm, and H. Gu, *Chem. Phys. Chem.* 13, 2016 (**2012**).
26. B. Chang, X. Zhang, J. Guo, Y. Sun, H. Tang, Q. Ren, and W. Yang, *J. Colloid. Interf. Sci.* 377, 64 (**2012**).
27. Y. Chen, H. Chen, S. Zhang, F. Chen, S. Sun, Q. He, M. Ma, X. Wang, H. Wu, L. Zhang, and J. Shi, *Biomaterials* 33, 2388 (**2012**).
28. T. Kim, E. Momin, J. Choi, K. Yuan, H. Zaidi, J. Kim, M. Park, N. Lee, M. T. McMahon, A. Quinones-HInojosa, and J. W. M. Bulte, *J. Am. Chem. Soc.* 133, 2955 (**2011**).
29. Z. Xu, Y. Gao, S. Huang, J. Lin, and J. Fang, *Dalton Trans.* 40, 4846 (**2011**).
30. S. Wu, Y. Huang, and C. Mou, *Chem. Commun.* 47, 9972 (**2011**).
31. J. M. Rosenholm, C. Sahlgren, and M. Lindén, *Current Drug Targets* 12, 1166 (**2011**).
32. A. Popat, S. Hartono, F. Sthar, J. Liu, S. Qiao, and G. Lu, *Nanoscale* 3, 2801 (**2011**).
33. J. M. Rosenholm, V. Mamaeva, C. Sahlgren, and M. Lindén, *Nanomedicine* 7, 111 (**2012**).
34. F. Tang, L. Li, and D. Chen, *Adv. Mater.* 24, 1504 (**2012**).
35. P. Yang, S. Gai, and J. Lin, *Chem. Soc. Rev.* 41, 3679 (**2012**).
36. Z. Li, J. C. Barnes, A. Bosoy, J. F. Stoddart, and J. I. Zink, *Chem. Soc. Rev.* 41, 2590 (**2012**).
37. E. von Haartman, H. Jiang, A. A. Khomich, J. Zhang, S. A. Burikov, T. A. Dolenko, J. Ruokolainen, H. Gu, O. A. Shenderova, I. I. Vlasov, and J. M. Rosenholm, *J. Mater. Chem. B* 1, 2358 (**2013**).
38. N. Prabhakar, T. Näreoja, E. von Haartman, D. ŞenKaraman, H. Jiang, S. Koho, T. A. Dolenko, P. E. Hänninen, D. I. Vlasov, V. G. Ralchenko, S. Hosomi, I. I. Vlasov, C. Sahlgren, and J. M. Rosenholm, *Nanoscale* 5, 3713 (**2013**).
39. Q. Cai, Z.-S. Luo, W.-Q. Pang, Y.-W. Fan, X.-H. Chen, and F.-Z. Cui, *Chem. Mater.* 13, 258 (**2001**).
40. K.-J. Lin, L.-J. Chen, M. R. Prasad, and C.-Y. Cheng, *Adv. Mater.* 16, 1845 (**2004**).
41. S. H. Joo, J. Y. Park, C.-K. Tsung, Y. Yamada, P. Yang, and G. A. Somorjai, *Nat. Mater.* 8, 126 (**2009**).
42. R. I. Nooney, T. Dhanasekaran, Y. Chen, R. Josephs, and A. E. Ostafin, *Adv. Mater.* 14, 529 (**2002**).
43. R. I. Nooney, D. Thirunavukkarasu, Y. Chen, R. Josephs, and A. E. Ostafin, *Langmuir* 19, 7628 (**2003**).
44. I. Gorelikov and N. Matsuura, *Nano Lett.* 8, 369 (**2008**).
45. H. Fan, J. Gabaldon, C. J. Brinker, and Y.-B. Jiang, *Chem. Commun.* 22, 2323 (**2006**).
46. P. Botella, A. Corma, and M. T. Navarro, *Chem. Mater.* 19, 1979 (**2007**).
47. X. Jiang and C. J. Brinker, *J. Am. Chem. Soc.*, 128, 4512 (**2006**).
48. M. Liong, B. France, K. A. Bradley, and J. I. Zink, *Adv. Mater.* 21, 1684 (**2009**).
49. J. Zhang, J. M. Rosenholm, and H. Gu, *Chem. Phys. Chem.* 13, 2016 (**2012**).
50. Q. Liu, J. Zhang, W. Xia, and H. Gu, *Nanoscale* 4, 3415 (**2012**).
51. Q. Liu, J. Zhang, W. Xia, and H. Gu, *J. Nanoscience and Nanotechnology* 12, 7709 (**2012**).
52. Y. Wang, J. Ren, X. Liu, Y. Wang, Y. Guo, Y. Guo, and G. Lu, *J. Coll. Interface Sci.* 326, 158 (**2008**).
53. J. Kim, H. S. Kim, N. Lee, T. Kim, H. Kim, T. Yu, I. C. Song, W. K. Moon, and T. Hyeon, *Angew. Chem. Int. Ed.* 47, 8438 (**2008**).
54. Y.-S. Lin and C. L. Haynes, *Chem. Mater.* 21, 3979 (**2009**).
55. P. Wu, J. Zhu, and Z. Xu, *Adv. Funct. Mater.* 14, 345 (**2004**).
56. W. Zhao, J. Gu, L. Zhang, H. Chen, and J. Shi, *J. Am. Chem. Soc.* 127, 8916 (**2005**).
57. Y. Deng, D. Qi, C. Deng, X. Zhang, and D. Zhao, *J. Am. Chem. Soc.* 130, 28 (**2008**).
58. W. Zhao, J. Shi, H. Chen, and L. Zhang, *J. Mater. Res.* 21, 3080 (**2006**).

59. W. Stöber, A. Fink, and E. Bohn, *J. Colloid Interface Sci.* 26, 62 **(1968)**.
60. C. Graf and A. van Blaaderen, *Langmuir* 18, 524 **(2002)**.
61. S. B. Yoon, J.-Y. Kim, J. H. Kim, Y. J. Park, K. R. Yoon, S.-K. Park, and J.-S. Yu, *J. Mater. Chem.* 17, 1758 **(2007)**.
62. J. H. Kim, S. B. Yoon, J.-Y. Kim, Y. B. Chae, and J.-S. Yu, *Coll. Surf. A: Physicochem. Eng. Aspects* 313, 77 **(2008)**.
63. T. Nakamura, M. Mizutani, H. Nozaki, N. Suzuki, and K. Yano, *J. Phys. Chem. C* 111, 1093 **(2007)**.
64. A. Guerrero-Martínez, J. Pérez-Juste, and L. Liz-Marzán, *Adv. Mater.* 22, 1182 **(2010)**.
65. N. Gibson, O. Shenderova, T. J. M. Luo, S. Moseenkov, V. Bondar, A. Puzyr, K. Purtov, Z. Fitzgerald, and D. W. Brenner, *Diamond Relat. Mater.* 18, 620 **(2009)**.
66. A. Pentecost, S. Gour, V. Mochalin, I. Knoke, and Y. Gogotsi, *ACS Appl. Mater. Interfaces* 2, 3289 **(2010)**.
67. A. Krueger, *J. Mater. Chem.* 18, 1485 **(2008)**.
68. V. N. Mochalin, O. Shenderova, D. Ho, and Y. Gogotsi, *Nat. Nanotechnol.* 7, 11 **(2012)**.
69. M. Ozawa, M. Inaguma, M. Takahashi, F. Kataoka, A. Krüger, and E. Îsawa, *Adv. Mater.* 19, 1201 **(2007)**.
70. O. A. Williams, J. Hees, C. Dieker, W. Jager, L. Kirste, and C. E. Nebel, *ACS Nano* 4, 4824 **(2010)**.
71. A. M. Scrand, S. A. C. Hens, and O. A. Shrenderova, *Crit. Rev. Solid State Mater. Rev.* 34, 18 **(2009)**.
72. A. Katiyar, S. Yadav, P. G. Smirniotis, and N. G. Pinto, *J. Chromatogr. A* 1122, 13 **(2006)**.
73. S. Liu, P. Cool, O. Collart, P. Van Der Voort, E. F. Vansant, O. I. Lebedev, G. Van Tendeloo, and M. Jiang, *J. Phys. Chem. B* 107, 10405 **(2003)**.
74. M. V. Korobov, D. S. Volkov, N. V. Avramenko, L. A. Belyaeva, P. I. Semenyuk, and M. A. Proskurnin, *Nanoscale* 5, 1529 **(2013)**.
75. S. Hens, S. Wallen, and O. Shenderova, U.S. Patent **(2009)**.
76. N. Petrova, A. Zhukov, F. Gareeva, A. Koscheev, I. Petrov, and O. Shenderova, *Diamond Relat. Mater.* 30, 62 **(2012)**.
77. E. Osawa, *Diamond Relat. Mater.* 16, 2018 **(2007)**.
78. G. W. Yang, J. B. Wang, and Q. X. Liu, *J. Phys.: Condens. Mater.* 10, 7923 **(1998)**.
79. S. Hua, F. Tian, P. Bai, S. Cao, J. Sun, and J. Yang, *Mater. Sci. Engg., B* 157, 11 **(2009)**.
80. L. Lai and A. S. Barnard, *J. Phys. Chem. C* 115, 6218 **(2011)**.
81. T. A. Dolenko, S. A. Burikov, J. M. Rosenholm, O. A. Shenderova, and I. I. Vlasov, *J. Phys. Chem. C* 116, 24314 **(2012)**.
82. A. Bumb, S. K. Sarkar, N. Billington, M. W. Brechbiel, and K. C. Neuman, *J. Am. Chem. Soc.* 135, 7815 **(2013)**.
83. E. K. Chow, X.-Q. Zhang, M. Chen, R. Lam, E. Robinson, H. Huang, D. Schaffer, E. Osawa, A. Goga, and D. Ho, *Sci. Transl. Med.* 3, 7321 **(2011)**.
84. X.-Q. Zhang, R. Lam, X. Xu, E. K. Chow, H.-J. Kim, and D. Ho, *Adv. Mater.* 23, 4770 **(2011)**.
85. K. K. Liu, W. W. Zheng, C. C. Wang, Y. C. Chiu, C. L. Cheng, Y. S. Lo, C. Chen, and J. L. Chao, *Nanotechnology* 21, 315106 **(2010)**.
86. R. A. Shimkunas, E. Robinson, R. Lam, S. Lu, X. Xu, X. Q. Zhang, H. Huang, E. Osawa, and D. Ho, *Biomaterials* 30, 5720 **(2009)**.
87. J. Li, Y. Zhu, W. Li, X. Zhang, Y. Peng, and Q. Huang, *Biomaterials* 31, 8410 **(2010)**.
88. A. H. Smith, E. M. Robinson, X. Q. Zhang, E. K. Chow, Y. Lin, E. Osawa, J. Xi, and D. Ho, *Nanoscale* 3, 2844 **(2011)**.
89. Y. Li, X. Zhou, D. Wang, B. Yang, and P. Yang, *J. Mater. Chem.* 21, 16406 **(2011)**.
90. B. Siddalingappa, V. Nekkanti, and G. V. Betageri, *OA Drug Design and Delivery* 1, 1 **(2013)**.
91. J. Li, X. Jiang, C. Ashley, and C. J. Brinker, *J. Am. Chem. Soc.* 131, 7567 **(2009)**.
92. J. M. Rosenholm, E. Peuhu, J. E. Eriksson, C. Sahlgren, and M. Lindén, *Nano Lett.* 9, 3308 **(2009)**.
93. J. M. Rosenholm and M. Lindén, *J. Control Release* 128, 157 **(2008)**.
94. V. Biju, T. Itoh, A. Anas, A. Sujith, and M. Ishikawa, *Anal. Biochem.* 391, 2469 **(2008)**.
95. D. Şen Karaman, D. Desai, R. Senthilkumar, E. Johansson, N. Råtts, M. Odén, J. E. Eriksson, C. Sahlgren, D. M. Toivola, and J. M. Rosenholm, *Nanoscale Research Lett.* 7, 38 **(2012)**.
96. C. O. Kim, S. J. Cho, and J. W. Park, *J Colloid. Interface Sci.* 260, 374 **(2003)**.
97. J. M. Rosenholm, A. Penninkangas, and M. Lindén, *Chem. Commun. (Camb.)* 3909 **(2006)**.
98. T. A. Dolenko, S. A. Burikov, K. A. Laptinskiy, T. V. Laptinskaya, J. M. Rosenholm, A. A. Shiryaev, A. R. Sabirov, and I. I. Vlasovn *J. Alloys Compd.* 586, S436 **(2014)**.
99. W. T. Godbey, K. K. Wu, and A. G. Mikos, *J. Controlled Release* 60, 149 **(1999)**.
100. O. Boussif, F. Lezoualc'h, M. A. Zanta, M. D. Mergny, D. Scherman, B. Demeneix, and J. P. Behr, *Proc. Natl. Acad. Sci. USA* 92, 7297 **(1995)**.
101. S. C. Hens, W. G. Lawrence, A. S. Kumbhar, and O. A. Shenderova, *J. Phys. Chem. C* 116, 20015 **(2012)**.
102. O. Shenderova, I. Vlasov, S. A. C. Hens, and V. Borjanovic, Enhancement of photoluminescence of nanodiamond particles; U.S. Patent Application 20100181534, ITC: USA, p. 28 **(2010)**.
103. O. Shenderova, S. Hens, I. Vlasov, S. Turner, Y.-G. Lu, G. Van Tendeloo, A. Schrand, S. A. Burikov, and T. A. Dolenko, Particle Part. Systems Character, DOI 10.1002/ppsc.201300251 **(2013)**.
104. D. R. Glenn, H. Zhang, N. Kasthuri, R. Schalek, P. K. Lo, A. S. Trifonov, H. Park, J. W. Lichtman, and R. L. Walsworth, *Sci Rep.* 2, 865 **(2012)**.
105. T. Zhang, H. Cui, C.-Y. Fang, L.-J. Su, S. Ren, H.-C. Chang, X. Yang, and M. Laird Forrest, *J. Biomed. Opt.* 18, 026018 **(2013)**.
106. Q. Zhang, V. N. Mochalin, I. Neitzel, I. Y. Knoke, J. Han, C. A. Klug, J. G. Zhou, P. I. Lelkes, and Y. Gogotsi, *Biomaterials* 32, 87 **(2011)**.
107. L. Zhou, Z. Li, Z. Liu, J. Ren, and X. Qu, *Langmuir* 29, 6396 **(2013)**.
108. T. Gulin-Sarfraz, J. Sarfraz, D. Şen Karaman, J. Zhang, C. Oetken-Lindholm, A. Duchanoy, J. M. Rosenholm, and D. Abankwa, *RSC Adv.* 4, 16429 **(2014)**.
109. D. Şen Karaman, T. Gulin-Sarfraz, G. Hedström, A. Duchanoy, P. Eklund, and J. M. Rosenholm, *Journal of Colloid and Interface Science* 418, 300 **(2014)**.

Received: 30 October 2013. Accepted: 3 January 2014.